Measurement of the ^{6}Li(n,α) neutron standard cross-section at the GELINA facility

Kaj Jansson[1,a], Ali Al-Adili[1], Riccardo Bevilacqua[2], Cecilia Gustavsson[1], Franz-Josef Hambsch[3], Stephan Pomp[1], and Marzio Vidali[3]

[1] *Department of Physics and Astronomy, Uppsala University, Box 516, 751 20 Uppsala, Sweden*
[2] *European Spallation Source, Box 176, 221 00 Lund, Sweden*
[3] *European Commission, Joint Research Centre, Institute of Reference Materials and Measurements (IRMM) Retieseweg 111-2440 Geel, Belgium*

Abstract. The ^{6}Li(n,α) reaction cross-section is commonly used as a reference cross section. However, it is only considered a neutron standard up to 1 MeV. For higher energies, there are discrepancies of several per cents between recent measurements and evaluated data files. In order to extend and establish ^{6}Li(n,α) as a neutron standard above 1 MeV these discrepancies must be resolved.
Our measurement at the GELINA facility at JRC-IRMM in Geel, Belgium is ongoing. We are using a double twin Frisch-grid setup to detect both α-particles from two ^{6}Li targets and fission products from two ^{235}U reference targets. Our targets have thick backings but are employed in pairs, one forward facing and one backward facing. In this way we still cover, in principle, a solid angle of 4π. We present some preliminary results showing that the existing cross-section data is well reproduced around the resonance at 240 keV. The final data taking will start in the beginning of 2016, when the GELINA facility goes online again after a few months of shut down.

1 Introduction

1.1 The cross section

The ^{6}Li(n,α) reaction cross-section is an established standard. One reason for that, is its relatively high cross section, while another reason is its high Q-value, of almost 5 MeV. A large Q-value enables the reaction products to give large clear signals in many detector setups, e.g. ionisation chambers. Depending on the setup, one or both of the product particles may be detected.

Currently, it is only considered a neutron standard up to 1 MeV. In order to extend and establish ^{6}Li(n,α) as a neutron standard above 1 MeV some issues must be resolved.

Up to 1 MeV the cross section from different experiments agree fairly well, but above 1 MeV to about 2.5 MeV discrepancies exist. The first resonance of ^{6}Li(n,α) occurs at a neutron energy of 0.240 MeV in the laboratory frame of reference. It corresponds to the $\frac{5}{2}^{-}$ excited state at 7.454 MeV in the compound nucleus [1]. Around 2 MeV three other levels in the compound nucleus contribute to

[a] e-mail: kaj.jansson@physics.uu.se

resonances in the ^{6}Li(n,α) reaction. However, their widths are much larger (4.71, 2.75 and 4.37 MeV compared to 0.080 MeV for the 7.454 MeV level) [1] and, therefore, the resonance structure is more smeared out.

In the 1-2.5 MeV region at least two independent experiments have reported discrepancies. One experiment was performed using an ionization chamber similar to the one used at JRC-IRMM (see Sect. 2.2) [2], while the second one employed solid state detectors [3]. Both experiments see a several percent higher cross section than, e.g., the ENDF/B-VII evaluation [4] in this energy region.

It is speculated [5] that one of the reasons the evaluation based on previous measurements shows a smaller cross section is the *Particle Leaking* effect. Due to the incoming neutron momentum there is a possibility of both products (t and α) being emitted in the forward direction (in the laboratory frame of reference), but with large polar angles ($\theta \lesssim 90^{\circ}$) for moderate neutron energies. In this case the detector response will look like as if only one particle, with the combined energy of both the triton and the α-particle, has entered the chamber. If this effect is overlooked it can lead to an underestimation of the cross section since the pulse height is much higher than for a normal α-particle event and might be discarded because of that. This is why the effect is called Particle Leaking.

The aim of this measurement is to allow for an extension of the standard energy range from 1 MeV to a few MeV. Therefore, any discrepancies in this region must be resolved before the cross section can be trusted as a standard.

2 Experimental setup

2.1 GELINA

The measurement is conducted at the *GEel LINear Accelerator* (GELINA) [6, 7] neutron source which resides at the *Joint Research Centre, Institute for Reference Materials and Measurements* (JRC-IRMM) in Geel, Belgium. It provides a pulsed continuous neutron energy spectrum that is peaked around 1-2 MeV but extends up to 20 MeV. To increase the neutron flux in the keV range a moderator is available.

The measurement of ^{6}Li(n,α) at GELINA is one out of three related experiments conducted at the JRC-IRMM. Detector setups similar to the one presented here have been used to measure ^{10}B(n,α)^{7}Li [8], also at the GELINA facility, and a measurement of the ^{6}Li(n,α)t cross section has been conducted at the VdG facility [9].

The experimental setup was viewing the neutron production target from a distance of 60 m. In the beginning of 2015 the setup was moved to a closer position (10 m) and was then also equipped with a moderated beam, in order to collect more data for lower neutron energies. The increased neutron flux at this distance allowed us to test modifications to the setup much quicker.

2.2 Gridded ionisation chamber

The detector setup consists of a twin Frisch-grid ionisation chamber which will measure the α-particles from the ^{6}Li(n,α)t reaction as well as the fission products from the ^{235}U(n,f) reference reaction. A schematic view of the *Gridded Ionisation Chamber* (GIC) is depicted in Fig. 1. The cylindrical chamber has one shared gas volume normally kept at a pressure slightly above 1 bar (the gas used was P-10), but the uranium measurement is confined to the front compartment of the chamber and the lithium measurement to the back. Targets with thick (0.5 mm) backings were used and two targets of ^{6}Li and ^{235}U respectively are employed in a back-to-back position in order to form a combined doubled sided target. The combined target in each compartment act as the cathode.

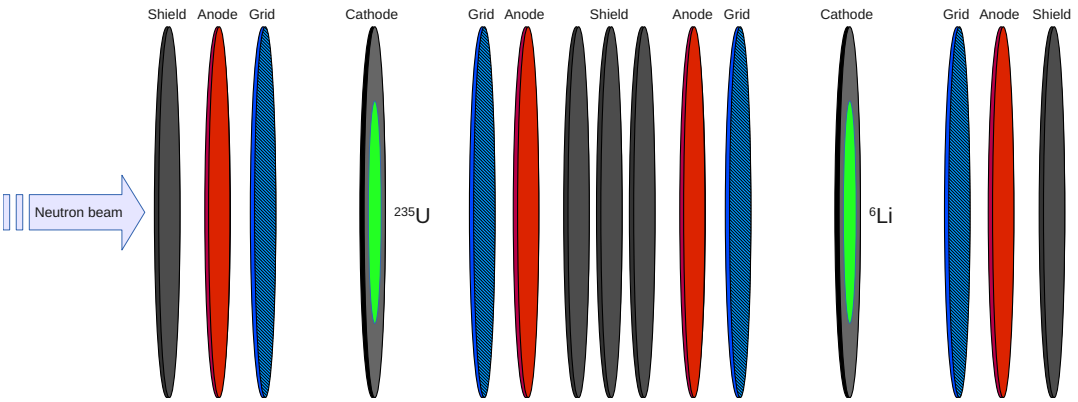

Figure 1. Schematic of the ionisation chamber. The chamber axis coincides with the neutron beam axis. Each cathode consists of two targets facing forward respectively backward. In total the chamber has 10 independent electrodes, five in each compartment separated by shields. The shields are interconnected and kept at the same potential.

Both lithium targets consisted of LiF, which was vacuum deposited on a aluminium backing and the deposited layers had similar masses, 2014 ± 23 and 2610 ± 40 µg, respectively. The 0.5 mm thick backings made it impossible for any reaction products to traverse the target to the other side of the cathode (the range of a 5 MeV triton in aluminium is only about 100 µm [10]). The uranium targets were of similar areal densities, 193 and 222 µg/cm^2, but due to different diameters they had different masses, 3071 ± 46 and 8520 ± 40 µg ^{235}U, respectively. The isotopic mass ratio of ^{235}U in the uranium target material were 97.663(3)% and 99.9336(14)% for the two targets, respectively.

On each side of each cathode, the chamber was equipped with an anode and a grid. The induced signals on each electrode were recorded by a 100 MHz digitiser. In theory one can calculate the third knowing two of the signals, but in practise it is better to record all of them in order to reduce uncertainties due to electronic drift [11]. The purpose of the grids is to shield the anodes and in this experiment they consist of conductive meshes (rather than parallel wires, which is another option).

What distinguish the gridded chambers from normal ionisation chambers is that the grids enable measurements of both particle energy and emission angle. The grid shields the anode from the ionisation electrons until they pass through it. The charge inducted on the anode will be independent on angle and proportional to the total number of electrons. On the grids however, the induced charge will be proportional to the cosine of the emission angle, θ. By treating the whole cloud of N electrons as a single charge, $-Ne$, and applying the Shockley-Ramo theorem [12] the total induced charges on the cathodes, anodes and grids can be derived as

$$Q_{\text{Cathode}} = -Ne\left(1 - \frac{\overline{X}}{D}\cos\theta\right) \tag{1}$$

$$Q_{\text{Anode}} = -Ne \tag{2}$$

$$Q_{\text{Grid}} = Ne\frac{\overline{X}}{D}\cos\theta, \tag{3}$$

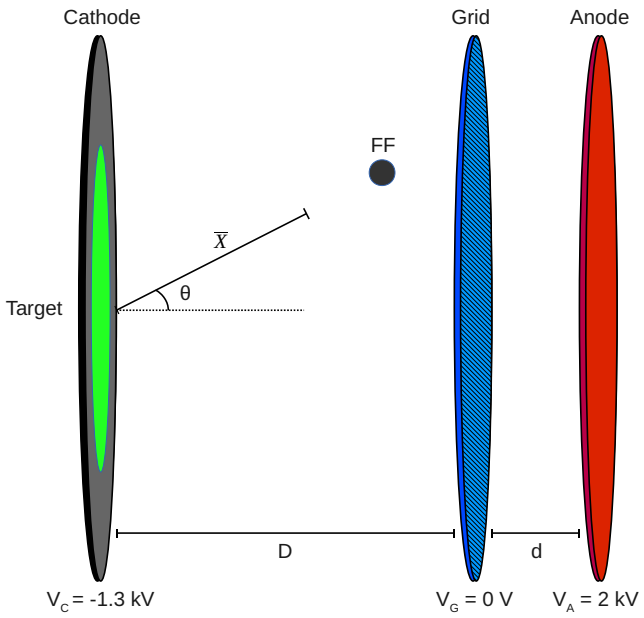

Figure 2. Schematic of the chamber electrodes. The emitted particle will leave a track of liberated electrons. The mean distance from the particle origin of these electrons is denoted $\overline{X}$. The grid-cathode distance, D, is 40 mm and the grid-anode distance, d, is 7 mm.

where $\overline{X}$ is the distance of the electron cloud's centre-of-gravity from the cathode along the particle track and D is the distance between the cathode and the grid. The notation is further illustrated in Fig. 2. For all types of signals we define the pulse height of the signal (PH) to be the digitised voltage level a short time after the event minus the voltage level right before the event (the baseline). The PH is therefore proportional to the total induced charge in Eq. 1-3.

These derivations were based on a perfect grid. In reality the grid will allow part of the electric field to leak through and therefore the anode is affected by the electrons even before they pass through the grid. The effect is in the order of a few percent and can be corrected for. A parametrisation of the so called grid inefficiency has been made by Göök et al., derived for different types of grids [13].

Since the last region the electrons will pass through is the one between the grid and the anode (the region where positive charge is induced on the grid), any loss of electrons will manifest itself as a more negative grid PH. In order for the electrons to pass through the grid without losses, the field strength between the grid and the anode must be several times higher than the field strength between the cathode and the grid. This has been investigated by Bevilacqua et al. [14] for mesh grids, which behave differently to parallel-wire grids.

3 Analysis

3.1 Signals

The digital sampling of the waveforms enables corrections in the post-analysis and has shown to be superior to analogue equipment [11]. However, the collection of stored waveforms needs to be iterated

in order to extract the relevant information. The parameters that are of interest, are in this case the time and the signal PH. To extract this information each signal was numerically fitted to a function consisting of line segments. Three segments, whereof two horizontal (four parameters in total), were used for cathode and anode signals while the grid signals required four segments (six parameters). The anode and grid signals from an α-particle event are depicted in Fig. 3 together with the corresponding fitted functions. The choice of fit function represents a compromise between the number of needed parameters, computation complexity and how well the function captures the signal features.

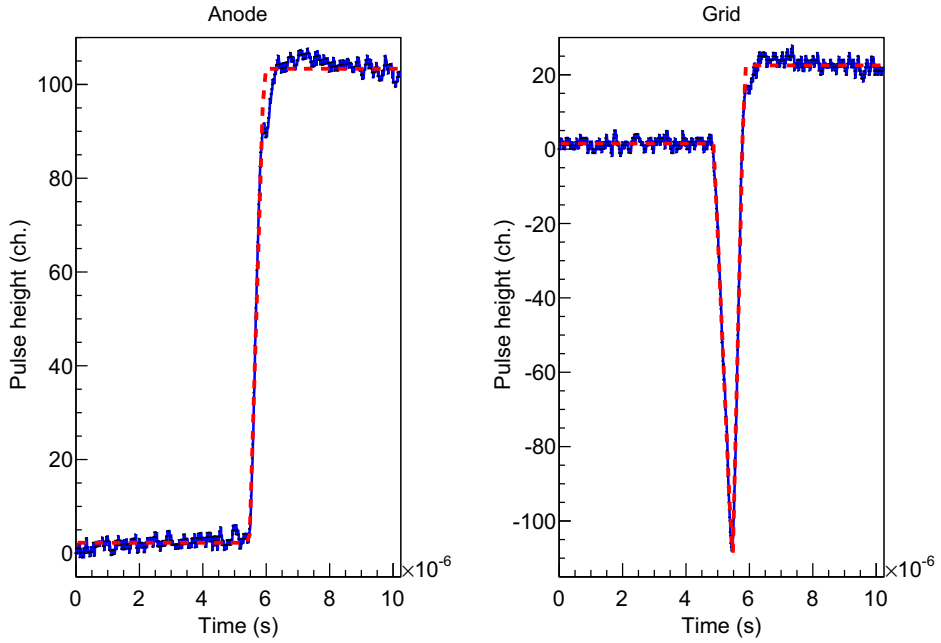

Figure 3. An example of anode and grid signals from an α-event. The anode signal in the left panel is easily distinguished from the grid signal in the right panel. The dashed lines represent the fits made to the signals.

By fitting the signals rather than just extracting the PH, more information become available, e.g. the signals' rise time. The deduced PHs from the fitted signals were compared to the PHs obtained by applying a noise reducing $CR\text{-}RC^4$ filter and then extracting the PH. No preference for either method could be seen. The χ^2-distribution from the fit results corresponded to the expected distribution considering the number of degrees of freedom as well as the uncertainty (noise) of the baseline.

3.2 Time-of-flight

The trigger was constructed by combining both cathode signals after they were fed through a CFD module. The recorded timestamp, t_{TS}, can be turned into the ToF, t_{ToF}, if a reference time, t_0, is known. The reference time can be found by observing the γ-flash coming from the neutron production target or by identifying resonances. The ToF is then given by,

$$t_{\mathrm{ToF}} = t_{\mathrm{TS}} - t_0 + L/c, \tag{4}$$

where L is the distance between the neutron production target and the relevant cathode. Once the neutron ToF is deduced the kinetic energy of the neutron, T_n, is given by:

$$T_n = m_n(\gamma - 1) = \frac{m_n}{\sqrt{1 - \frac{L^2}{t_{\mathrm{ToF}}^2 c^2}}} - m_n, \tag{5}$$

where $m_n = 939.565379\,\mathrm{MeV}$ is the neutron mass.

We observed a correlation between the anode PH and the ToF when t_{TS} was used without any correction. Since all signals were digitised, we could correct the timestamp based on an extrapolation of the slope of the cathode signal to the baseline. This procedure removed the time walk completely.

Bismuth and lead plates were placed in the neutron beam in front of the chamber during the measurements, in order for resonances to be visible in the ToF spectrum. Unfortunately, the statistics has not been enough in order to resolve and identify most of them. The resonance structure of ^{235}U can serve the same purpose as the beam filters. In this case many peaks have been identified and were used to calibrate the ToF in the eV to keV region.

Even though piled up events are rare in our data, we have implemented a routine that searches for such events. This is done by analysing the differentiated signal. If the piled up signals can be resolved the routine is also able to correct the digitised signal by removing one of the signals. The removal is performed by setting the derivative to zero in the region where the piled up event resides and integrating.

3.3 Fission events

Due to the much larger energy deposited in the gas by FFs, a PH threshold separated the FFs unambiguously from the α-particles. Due to the backing thickness, only one of the two FFs is detected for each fission event. The mass of the FF is, for each single event, unknown and can only be estimated based on its energy. The neutron energy does not reach more than a few MeV, so its influence on the fragment kinematics will be small.

The analysis starts by plotting the grid PH versus the anode PH as in Fig. 4. For each anode channel the fission events are projected onto the grid axis. The projection is used to determine for which grid values the distribution drops to half its maximum. These grid values, G_0 and G_1, correspond to $\cos\theta = 0$ and $\cos\theta = 1$ (or $\cos\theta = -1$ for particles emerging from the backwards facing target). From Eq. 3 it is known that the grid signal is proportional to $|\cos\theta|$ which allows us to derive the following formula:

$$|\cos\theta| = \frac{G(Q_G) - G_0}{G_1 - G_0}. \tag{6}$$

The value of G_0 is always very close to zero but the value of G_1 will change with the fragment energy since it incorporates $\overline{X}$ which in turn depends on the stopping range of the heavy ion in question. It turns out that G_1 can be well parametrised by two line segments as shown in Fig. 4.

The fragments emitted in an angle close to 90° will suffer from larger energy losses in the target since the effective thickness of the target is proportional to $\frac{1}{\cos\theta}$. Corrections for the energy losses in the target can be made by observing the mean energy of all events for a certain cosine value. The inverse cosine is plotted against the anode PH, A, and a straight line, $A = \frac{k}{|\cos\theta|} + m$, is fitted to the data where the losses are not too big. We can estimate the anode PH, in the absence of energy loss in the target, with

$$A_{\text{no loss}} = A(\theta) - \frac{k}{|\cos\theta|}, \tag{7}$$

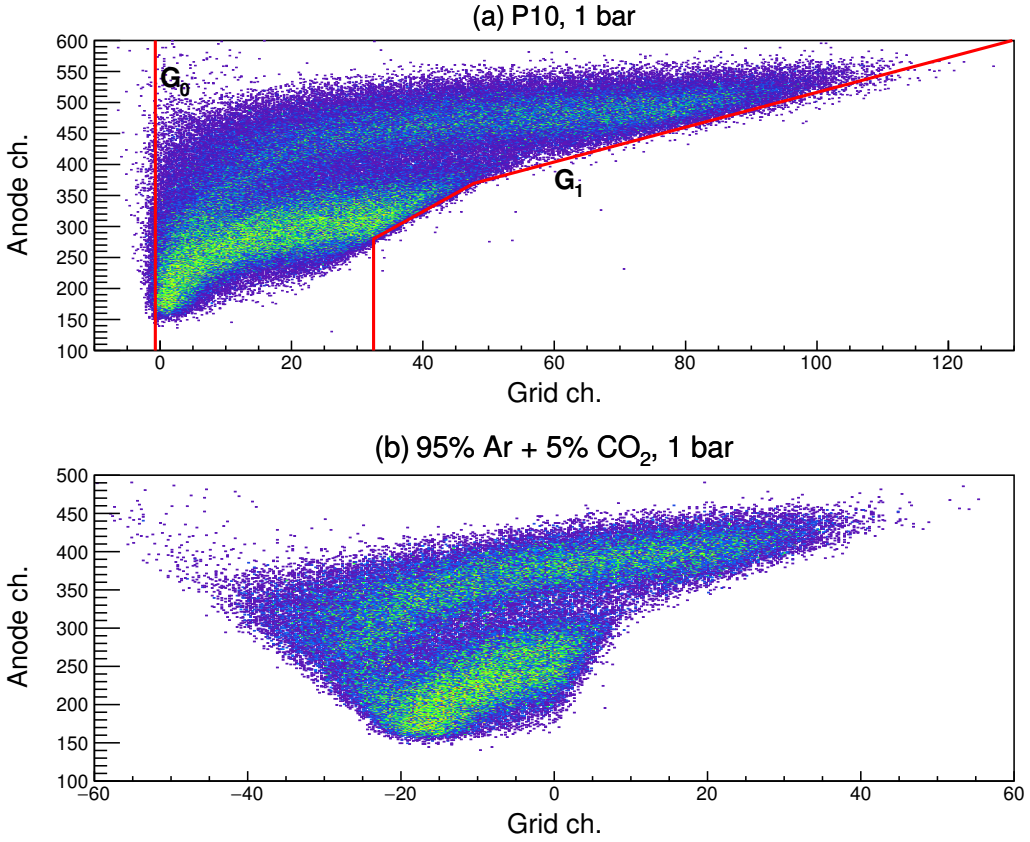

Figure 4. The top panel (a) shows the grid signal PH plotted against the anode signal PH, for all fission events in the forward direction when using P10 as the ionisation gas. The lines represent the limits G_0 and G_1 (see Eq. 6), where the distribution height drops to half its maximum and defines $\cos\theta = 0$ and $\cos\theta = \pm 1$. The bottom panel (b) shows the same plot but with 95% Ar + 5%CO_2 as the ionisation gas. The extensive negative grid signals in this case shows that the two gases have quite different properties when it comes to electron losses, if the same electric potentials are used.

through extrapolation of the fitted line by letting $\frac{1}{\cos\theta} \to 0$. For gracing angles the energy losses are too big to be well corrected for and some particle losses are unavoidable, for the final results only the events with $|\cos\theta| > 0.3$ are used currently.

As previously mentioned the reduced field strengths, both between cathode and grid as well as between grid and anode, are important parameters. The kind of gas and the type of grid determines how, e.g., drift velocity, recombination and electron captures are affected by the pressure and voltage settings. Negative grid PHs can be a sign of a bad configuration and often indicate electron losses. More investigations like the one in ref. [14] are needed.

3.4 Lithium events

The two reaction products (^{4}He and ^{3}H) have comparable masses to the neutron's, which means that the kinematics are strongly dependent on both the neutron energy and the emission angles in

the laboratory frame of reference. For all, except very low, neutron energies the two products will not be emitted in opposite directions (in the laboratory frame of reference) due to the momentum transfer of the incoming neutron. One effect of this is the *Particle Leaking* which was discussed in the Introduction.

The anodes can be calibrated by installing an α-particle source but this has not yet been done. Instead the only way of determining the deposited energy is by kinematical calculations based on the neutron energy. The α-particle emission angle is determined analogously to how it was done for the fission fragments. To be able to do kinematic calculations and transform the system into the centre-of-momentum (CoM) frame, the anodes must be calibrated. This was done by calculating the theoretical α-particle energy using the neutron energy determined by the ToF technique at $\cos\theta = 0$ and $\cos\theta = \pm 1$. The two end points had to be independently calibrated since the energy loss in the target does not scale linearly with particle energy. The laboratory energy were determined for each event by interpolation between the two end point calibrations.

Once the laboratory properties of the α-particle are known they can be transformed into the CoM frame by Lorentz transformation and energy and momentum conservation. One finds that

$$T_\alpha^* = \gamma\left(E_\alpha - \beta\cos\theta\sqrt{E_\alpha^2 - m_\alpha^2}\right) - m_\alpha \tag{8}$$

$$\cos\theta^* = \pm\sqrt{1 - \frac{E_\alpha}{E_\alpha^*}(1 - \cos^2\theta)}, \tag{9}$$

where E denotes total relativistic energy, T denotes kinetic energies, m denotes mass and all CoM properties are marked by *. The negative solution in Eq. 9 is applied for the backward facing side while the positive is applied for the forward facing side. In addition $\cos\theta^*$ is multiplied by -1 if $\cos\theta_{\text{limit}} > \cos\theta$ where θ_{limit} is given by

$$\theta_{\text{limit}} = \arctan\sqrt{\frac{(m_n + m_{\text{Li}})^2}{m_n m_\alpha}\frac{m_t}{m_\alpha + m_t}\frac{E_n + Q}{E_n}}, \tag{10}$$

in order to take into account that the forward laboratory angle might have reached into the back hemisphere of the CoM frame.

4 Preliminary results

4.1 Fission spectra

The result of changing the P10 gas to 95% Ar+5% CO_2 was lots of events with negative grid PHs (see Fig. 4). Properties that can affect the electron losses, like the electron drift velocity and temperature as well as recombination and capture rates, are not the same for the two gases. The new argon mixture needed higher voltage settings. However, our high-voltage supplies were already operated close to their maximum setting so a switch back to P10 was made, since proper settings for this gas could be obtained.

For FFs of gracing angles, the effective thickness of the target becomes large. Consequently, the energy losses will be large too, making accurate corrections more difficult. Sometimes the fragments will not even escape the target. One can see that some losses of events are occurring in the cosine spectra in Fig. 5.

To avoid being affected by particle losses, currently only the fission events where $|\cos\theta| > 0.3$ are used. The ratio of event counts in the forward and backward direction was compared to the ratio of ^{235}U atoms in the corresponding targets and the difference to the expected value was 1.2%.

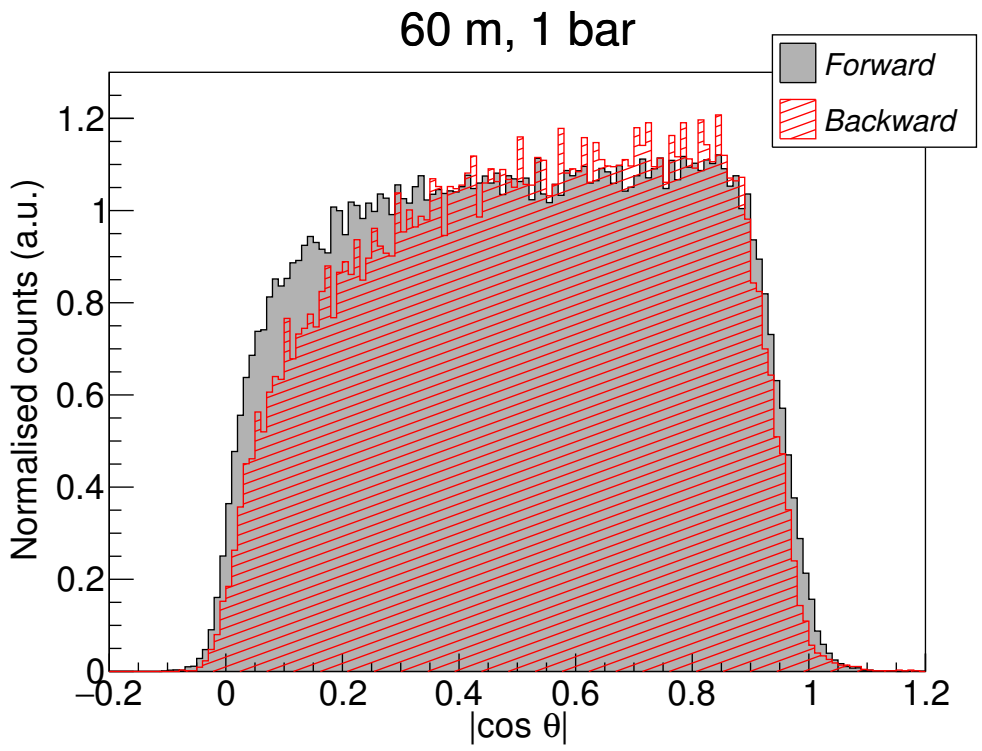

Figure 5. Cosine distributions of the events emerging from the forward and backward facing fission targets respectively. The data comes from the measurement at 60 m distance and 1 bar pressure. When $|\cos\theta| \lesssim 0.3$ the energy losses in the target soon become large and in the backward direction one sees a larger loss of events due to this. We see systematically broader distributions from the older target (here put in the backward position) which has smaller diameter and is slightly thinner. The spectra have been normalised based on the events where $|\cos\theta| > 0.3$. Apart from losses due to the target, the distributions are quite well aligned and somewhat isotropic.

Depicted in Fig. 6 are the two energy spectra from the forward and backward directions. They match each other well, but some small discrepancies can be seen at lower energies.

4.2 Preliminary cross section

A preliminary cross section has been calculated and compared to the ENDF/B-VII.1 evaluation [4] (see Fig. 7). The experimental cross section shows a tendency of being systematically too low except for low energies, but around the resonance region the agreement is fairly good. The measured cross section peaks at 243 keV, close to the expected energy. With better statistics the binning can be made finer and the neutron-energy is expected to improve when more resonances are utilized in the ToF calibration (see Sect. 3.2).

For energies below ~150 keV or above 1 MeV large systematic differences to the evaluation are seen. In the low energy region the measurement overestimates the cross section due to a troublesome background. The origin of this background is, by the time of writing, unknown. Also for the higher energies a cluster of background events partly overlaps with the α-particle distributions making it difficult to correctly select the appropriate events. However, it is less severe than for the lower energies.

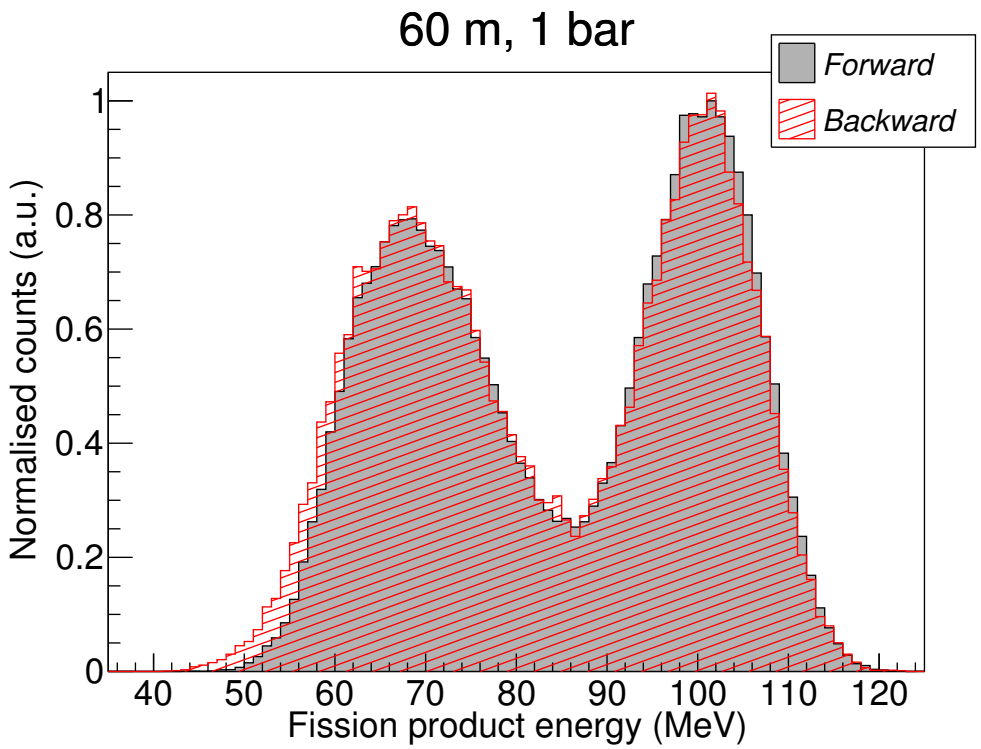

Figure 6. Anode energy spectra for events with $|\cos\theta| > 0.3$ from the data taken at 60 m distance and 1 bar pressure. The two peaks in each spectrum were used to roughly calibrate the x-axis and were positioned at 68 and 101 MeV, respectively, based on GEF calculations [15] of the thermal fission of ^{235}U. Both spectra were normalised with respect to the number of ^{235}U atoms in their respective target. We see a low energy tail from the older target (here put in the backward position) which has smaller diameter and is slightly thinner.

Part of the underestimation of the cross section at higher energies can be explained by the Particle Leaking effect, discussed earlier in Sect. 1.1, which becomes more important the higher the neutron energy is. It has not yet been corrected for.

4.3 Improving the experimental conditions

During 2015 the whole setup was moved to a shorter flightpath of about 10 m. This allowed us to gather statistics and identify problems much faster since the neutron flux is more than an order of magnitude larger at the shorter distance. At the new position the background situation, for both low and high energies, seems to have changed and does not disturb the α-distributions as much as at the 60 m position. A comparison of the 10 m data to the ENDF cross section was not possible due to a misalignment of the chamber that was not discovered in time to correct it before the accelerator stopped, in June 2015.

If a 1 bar pressure is used with the setup it will not fully stop all the tritons while a 2 bar pressure will do the trick. The events that was caused by neutrons of similar energies (similar ToF) were analysed together which allows for identifying the different ion species as band shaped clusters in a

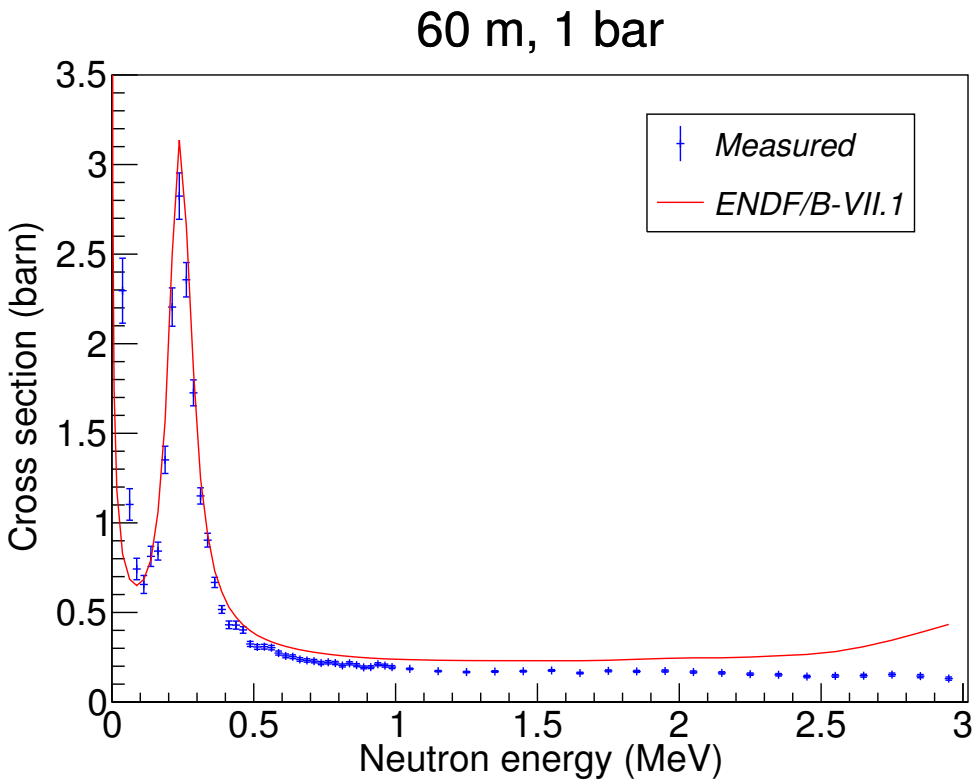

Figure 7. Preliminary cross section of the ^{6}Li(n,α) reaction, the error bars represent statistical uncertainties only. To obtain absolute values the ^{235}U cross section from the ENDF/B-VII.1 evaluation [4] has been used. The measured fission counts have been extrapolated in the $|\cos\theta| \in [0, 0.3)$ region assuming an isotropic emission. Agreement in the low and high energy region is not so good but around the resonance region our measured data agrees well with the evaluation. Only data from the 60 m measurement was used due to a misalignment of the chamber at 10 m.

grid-versus-anode plot (see Fig. 8). The partially stopped tritons can sometimes interfere with the α-particle distribution and this is why the pressure was increased to 2 bar. Fully stopping the tritons also leaves more available information for the analysis. Unfortunately, we also seem to get more negative grid signals for the α-particles and the fission fragment distribution became distorted due to the higher energy losses in the ionisation gas.

5 Conclusion and outlook

Although some problems remain, the analysis of the 60 m data has been able to replicate the evaluated ^{6}Li(n,α) cross section from ENDF/B-VII.1 [4] in the energy region from hundreds of keV to about 1 MeV. The prominent issues were mainly background related although upon moving the whole setup to a different location, closer to the neutron production, the background became less problematic.

The linear accelerator was shut down in July (2015) and will start again in beginning of 2016. Then we plan to have two separate chambers that we will be placed at 30 m distance from the source.

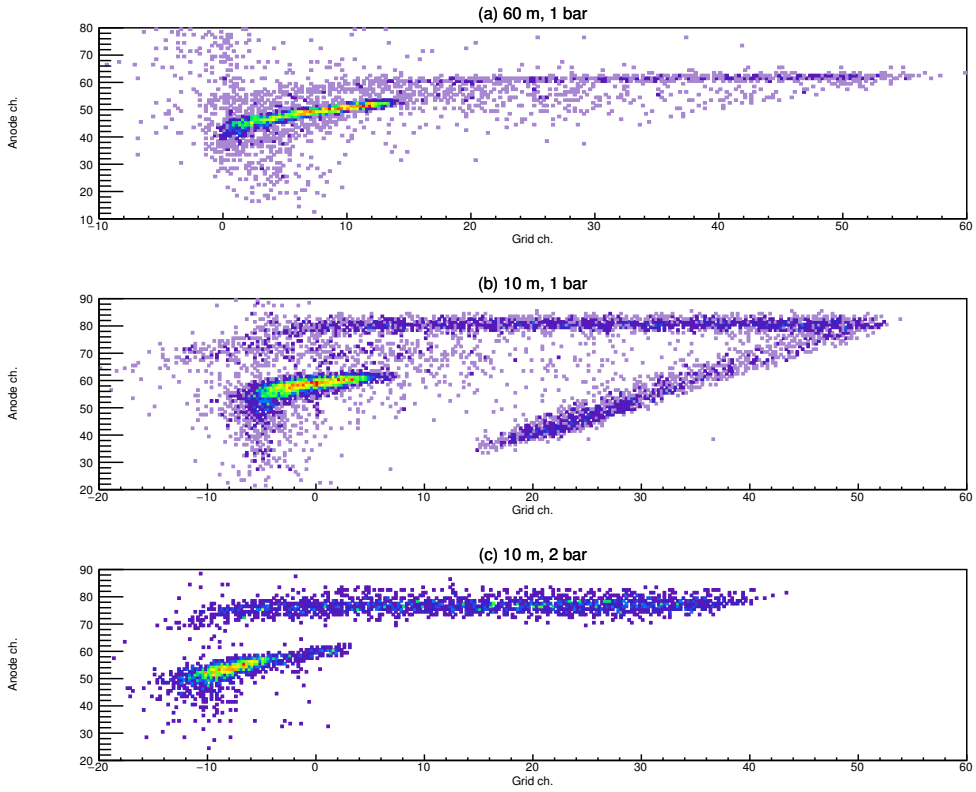

Figure 8. Forward directed events from the Li target. The top panel, (a), shows the neutron energy interval 200-250 keV from the measurement at 60 m distance and 1 bar pressure. The lower panels, (b) and (c), show similarly the neutron energy interval 6-7 keV from the measurement at 10 m distance at 1 bar and 2 bar pressure, respectively. The lower cluster of events in each panel, respectively, are α-particles. The top cluster are tritons which are only partly stopped when the chamber pressure is 1 bar. The α-particle distribution is bent due to both the frame boost and to energy losses in the target. In the middle panel, (b), some CFD thresholds had been adjusted and therefore the punch-through kink is clearly seen in (b) but not in (a). By fully stopping the tritons much less events fall between the two clusters.

The Li chamber will have a higher pressure in order to also stop tritons while the U chamber will keep the current pressure of about 1 bar.

References

[1] D. Tilley, C. Cheves, J. Godwin, G. Hale, H. Hofmann, J. Kelley, C. Sheu, H. Weller, Nuclear Physics A **708**, 3 (2002)
[2] G. Zhang, J. Chen, G. Tang, Y. Gledenov, M. Sedysheva, G. Khuukhenkhuu, Nucl. Instrum. Meth. A **566**, 615 (2006)
[3] M. Devlin, T.N. Taddeucci, G.M. Hale, R.C. Haight, J.M. O'Donnell, AIP Conference Proceedings **1090**, 215 (2009)

[4] M. Chadwick, M. Herman, P. Obložinský, M. Dunn, Y. Danon, A. Kahler, D. Smith, B. Pritychenko, G. Arbanas, R. Arcilla et al., Nuclear Data Sheets **112**, 2887 (2011), special Issue on ENDF/B-VII.1 Library
[5] R. Bencardino, R. Bevilacqua, G. Giorginis, F.-J. Hambsch, Nucl. Sci. Eng. **177**, 68 (2014)
[6] Institute for Reference Materials and Measurements (Geel), Unit Standards for Nuclear Safety, Security and Safeguards, *EUFRAT NUCLEAR FACILITIES AT JRC-IRMM*, Accessed: 2015-03-10, https://ec.europa.eu/jrc/sites/default/files/eufrat-facilities.pdf
[7] European Commission, Joint Research Centre, *Linear electron accelerator facility*, Accessed: 2015-03-10, https://ec.europa.eu/jrc/en/research-facility/linear-electron-accelerator-facility
[8] F.J. Hambsch, I. Ruskov, Nucl. Sci. Eng. **163**, 1 (2009)
[9] R. Bevilacqua, F.-J. Hambsch, R. Bencardino, G. Giorginis, M. Vidali, L. Lamia, I. Ruskov, Nuclear Data Sheets **119**, 104 (2014)
[10] J.F. Ziegler, M. Ziegler, J. Biersack, Nucl. Instrum. Meth. B **268**, 1818 (2010), 19th International Conference on Ion Beam Analysis
[11] A. Al-Adili, F.-J. Hambsch, S. Oberstedt, S. Pomp, Sh. Zeynalov, Nucl. Instrum. Meth. A **624**, 684 (2010)
[12] W. Shockley, Journal of Applied Physics **9**, 635 (1938)
[13] A. Göök, F.-J. Hambsch, A. Oberstedt, S. Oberstedt, Nucl. Instrum. Meth. A **664**, 289 (2012)
[14] R. Bevilacqua, A. Göök, F.-J. Hambsch, N. Jovančević, M. Vidali, Nucl. Instrum. Meth. A **770**, 64 (2015)
[15] K.H. Schmidt, B. Jurado, C. Amouroux, Tech. Rep. 24, Nuclear Energy Agency (2014)